Available free online at www.medjchem.com

Mediterranean Journal of Chemistry **2022**, 12(1), 83-99

Experimental, DFT studies, and *in silico* molecular docking investigations of (Z)-2-amino-4-(methylthio)-N-phenylbutanehydrazonic acid and its Fe(II) and Mn(II) metal complexes as a potential antibacterial agent

Terkumbur E. Gber [1, 2, *], Onyinye J. Ikenyirimba [1, 3], Benjamin E. Etinwa [1, 2], Immaculata J. Ikot [1, 2], Imabasi T. Ita [1, 2], Chioma M. Chima [1, 2], Ismail O. Amodu [1, 4], Bartholomew B. Isang [1, 4], Innocent Benjamin [a, *] and Grace Iniama [1, 2]

[1] Computational and Bio-Simulation Research Group, University of Calabar, Calabar, Nigeria

[2] Department of Pure and Applied Chemistry, Faculty of Physical Sciences, University of Calabar, Calabar, Nigeria

[3] Department of Chemistry Education, Alex Ekwueme Federal University Ndufu-Alike, Ebonyi State, Nigeria

[4] Department of Mathematics, Faculty of Physical Sciences, University of Calabar, Calabar, Nigeria

Abstract: Metal complexes of Methionine-phenylhydrazone (MPH) Schiff base were synthesized and experimentally characterized using FT-IR and UV-vis spectroscopy. The synthesized structures: MPH, $Fe(MPH)_2T_2$, and $Mn(MPH)_2T_2$ were theoretically studied using advanced electronic structure theory based on density functional theory (DFT) using the B3LYP and LanL2DZ methods. From the FT-IR spectral results, the ligand was bidentate coordinated to the central metal ion through the nitrogen atom of the azomethine group and the oxygen atom of the carbonyl group. As observed, the octahedral configuration of the molecule was due to the incorporation of the monodentate secondary ligand thiophene. The HOMO-LUMO results reveal the energy gap of $Fe(MPH)_2T_2$ and $Mn(MPH)_2T_2$ to be 3.39 eV and 2.83 eV, respectively. $Fe(MPH)_2T_2$ was observed to have the highest energy gap, which shows that it is a hard and energetically stable molecule relative to $Mn(MPH)_2T_2$, which is softer and more reactive than $Fe(MPH)_2T_2$. The topological analysis of the complexes reveals the $Mn(MPH)_2T_2$ complex with the relatively highest coordination bond based on the electron density distribution between the ligand and the metal atom. The experimental and computational drug design analysis shows the potential of the studied compounds as antibacterial agents. The molecular docking results reveal that the synthesized complexes generally showed greater interaction with 2XCS receptor proteins with significant hydrogen bond interactions and better binding affinity of -7.1, -9.3, -8.4 Kcal/mol for MPH, Mn(MPH)2T2, and Fe(MPH)2T2 respectively.

Keywords: Schiff base; metal complex; synthesis; characterization; DFT; molecular docking.

1. Introduction

Schiff Bases are nitrogen analogs of aldehydes and ketones in which the carbonyl has been replaced by an imine or azomethine group [1]. This reaction results in the elimination of water molecules and are said to be a condensation reaction. Schiff bases are easily synthesized structurally and form complexes with almost all metal ions. The common structural feature of this compound is the imine or the azomethine functional group (-C=N-) [2]. In azomethine derivatives, the (-C=N) linkage is essential specifically for molecular interactions as several azomethines have been reported to possess remarkable antibacterial, antifungal, anticancer and antimalarial activity [3,4]. Schiff base ligands with oxygen or nitrogen donor atoms are a promising class of organic compounds capable of binding to different metal ions with interesting medicinal and non-medicinal properties. They also display great biological activities such as antioxidant, antimicrobial, antidiabetic, and anticancer. They are excellent chelating agents due to the presence of potential donor sites. Meta chelation can tremendously influence organic ligands' antimicrobial/bioactive behavior [5]. Schiff bases are essential in the field of coordination chemistry, especially in the development of complexes of transition metal ions due to their ability to form highly stable complexes [6]. They are used in optical and electrochemical sensors and in various

**Corresponding author: Terkumbur E. Gber; Innocent Benjamin*
Emails: gberterkumburemmanuel@gmail.com, Innocentbenjamin53@gmail.com
DOI: http://dx.doi.org/10.13171/mjc02207301640gber

Received June 23, 2022
Accepted July 16, 2022
Published July 30, 2022

chromatographic methods to enable detection due to enhanced selectivity and sensitivity.

Researchers have developed much interest in theoretical or computational analysis to support or confirm experimental results. Computational methods help investigate or identify the proposed geometry of compounds, the nature of chemical bonds, and the type of intermolecular or intramolecular interaction present in molecules with high or dependable accuracy [7]. Different theoretical methods have been developed, which are helpful for analyzing the complex bonding nature of metal complexes. One of such methods is the quantum theory of atoms in a molecule (QTAIM). The QTAIM based on topological analysis of electron density, allows chemists to grasp, anticipate and interpret experimental results intuitively. A comprehensive characterization of the metal-ligand and metal bonding was carried out by examining the topology of electron density within the QTAIM [8,9] and the delocalization of electrons within the complexes. NBO analysis was used to analyze the intra and intermolecular bonding and also provides a convenient basis for investigating charge transfer or conjugative interaction in molecular systems [10-12]. More so, the HOMO-LUMO energy values and quantum reactivity descriptors were exploited to calculate the critical quantum chemical parameters of the reactivity and stability trend of the compounds under investigation [13,14].

Thus, owing to the copious merit of Schiff bases and their numerous biological applications, they have focused on designing and modeling novel potent compounds as potential antibacterial agents. As such, this present work sought to present the detailed synthesis, spectroscopic (UV-vis and FT-IR) characterization, DFT studies, and the theoretical modeling of metal complexes of Methionine-phenylhydrazone Schiff as potential drug candidates for the management of bacterial infection. Geometric optimization and theoretical assignment of the UV-vis spectra of the ligand were obtained appropriately by employing DFT calculations to give a systematic theoretical insight and compare the experimentally obtained results with calculated data. In addition, in silico molecular docking studies were equally carried out to assess the suitability of the studied complexes as potential drug candidates and match the experimental antimicrobial data with theoretical insights.

2. Materials and methods

2.1. Experimental details

All chemicals were purchased from Sigma Aldrich and used without further purification. Shimadzu FTIR-8400S, FT-IR spectra were performed on Perkin-Elmer model 240 spectrometer automatic elemental analyzer, Spectro UV-vis double beam PC scanning spectrophotometer (UVD2960) was used for UV-VIS spectra, Jenway 4510 conductivity bridge with conventional dip- type black electrode, Gallenkemp melting point apparatus autoclave, nutrient agar, potato dextrose sugar uniscope SM 9053, wire loop and paper discs were also utilized for the experimental analysis, correspondingly.

2.2. Synthesis of methionine-phenylhydrazone ligand

Phenylhydrazone (0.001 mol, 0.108 g) in 20 ml ethanol was mixed with methionine solution (0.001 mol, 0.149 g) in 20 ml ethanol and stirred for 3 minutes using a magnetic stirrer. Next, five drops of glacial acetic acid were added and mixed with a magnetic stirrer for 2 hours. The solution was allowed to stand overnight. Finally, the white precipitate formed was filtered, washed with ethanol, recrystallized with hot methanol, and dried over fused calcium chloride in desiccators [15].

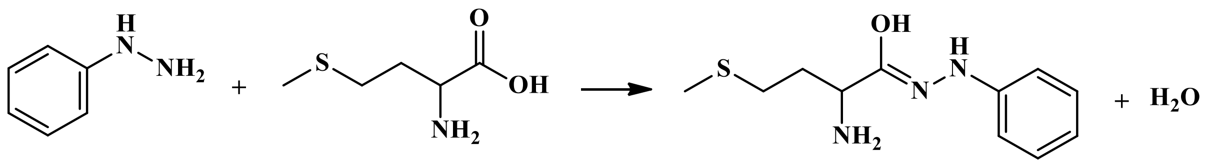

Figure 1. Synthesis of the primary ligand

2.3. Synthesis of Metal mixed ligand complex

A solution of Fe (III) chloride (0.001 mol, 0.162 g) in 20 ml ethanol was added to the synthesized methionine-phenylhydrazone (0.001 mol, 0.239 g) and stirred for 15 minutes; 20 ml of thiophene was added and stirred 2 hours. The brown precipitate formed was filtered, washed with ethanol, recrystallized with hot methanol, and dried over fused calcium chloride in a desiccator. The procedure was repeated with Mn (II) chloride [16].

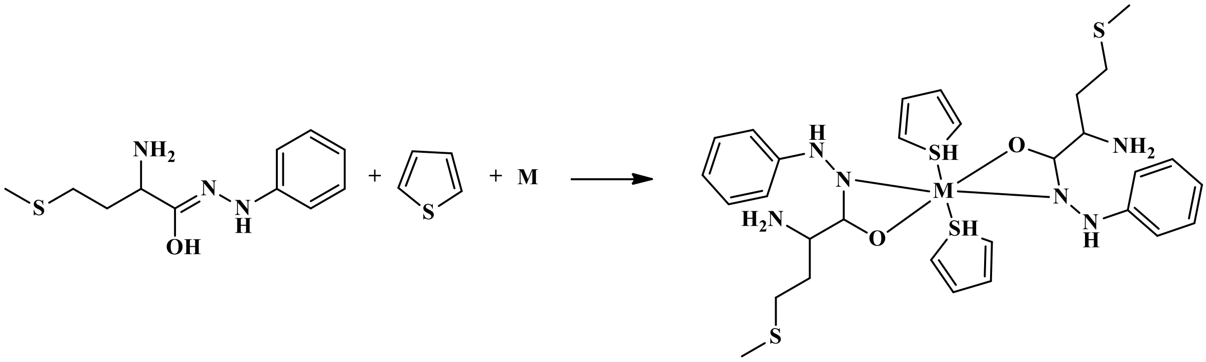

Figure 2. Synthetic route of Metal complex

2.4. Computational methods

2.4.1. Density functional theory (DFT) computation

Computational calculations have been carried out using the Gaussian09W and GaussView 6.0.16 softwares [17,18] within the density functional theory electronic structure method framework. The general basis (gen) along with the 6-311++G(d,p) and the LanL2DZ basis set was used for the lighter (H, C, S, O, and N) and heavy elements, respectively. The Natural Bond Orbital (NBO) calculations were conducted using NBO 3.1 module embedded in Gaussian09W. All frontier molecular orbital (HOMO and LUMO) isosurface maps were plotted using the checkpoint files from the optimized geometry; meanwhile, quantum theory of atoms-in-molecules (QTAIM) investigations were carried out using Multiwfn 3.7 dev software [19].

2.4.2. Molecular docking approach

The studied compounds were utilized as ligands of interest (substrates) in the molecular docking assay to investigate their binding affinity against the *E. coli* 2,2-dialkylglycine decarboxylase (PDB ID:1D7U) and *S. Aureus* DNA Gyrase (PDB ID:2XCS) proteins. Consequently, the molecular docking simulation obtained 3D structures of the protein complex (PDB code: 1D7U and 2XCS) from the Research Collaboratory for Structural Bioinformatics (RCSB) website. The proteins were prepared using the Biovia discovery studio 4.5 software, and docking was then performed using AutoDock vina 4.2 [20]. The 3D and 2D metal-ligand interaction as well as the H-bond interaction was visualized using the Biovia discovery studio [21]. The ability of the selected proteins (residue) to recognize the substrate and the presence of the significant cavity around the active site may account for this enzyme activity to bind with the studied complexes. Also, according to the literature review, it was observed that the two proteins could form the catalytic pair as those conserved in the studied compound. On the other hand, the mechanism for immune system suppression and the guided mutations of the protein shows that the protein binds to the residues essential for the mediation and detection of microbial infection is hence providing the snapshot of an ongoing molecular arms race between the protein and the studied structure which result in the choice of proteins1D7U and 2XCS respectively. The ligands (complexes) used for docking were subjected to pre-geometry optimization using the molecular mechanic optimization with MM+ force field implemented in the HyperChem program [22] has been performed on model structures and outputs used for the molecular docking.

3. Results and Discussion

Table 1a lists the physical parameters of the produced substances. The qualities are color, physical nature, melting points, and molar conductivity. Colors range from white to brown to pink. The ligand was crystalline in form, whereas the complexes were powdery. All the compounds were stable in the presence of air but melted at relatively high temperatures (268ºC-289ºC), implying that the chelates were not in their pure form but rather in polymeric forms [23]. Their color changed as they decomposed, indicating that they melted. The non-electrolytic character of the complexes was reflected in the low molar conductivity values of 0.72 Ω cm^2 mol^{-1} – 0.93 Ω cm^2 mol^{-1}. The antibacterial activity of the ligand and mixed ligand complexes was tested on gram-positive bacteria *Staphylococcus aureus*, gram-negative bacteria *Escherichia coli*, and fungus Candida albican and Aspergillus niger. Table 1b shows the data for the zones of inhibition for the bacteria mentioned above. The ligand has a smaller zone of inhibition than the chelates, consistent with the findings of [24,25]. On S. aureus, for example, the Mn(II) complex has a 15mm inhibition zone, while *E. coli* has a 12mm inhibition zone. The zone created by the Fe(III) complex measured 12mm against *S. aureus* and 11mm against *E. coli*, but the zone caused by the ligand was only 8mm for both bacteria. The average zone for the fungi was 10mm for the two fungi. These restriction zones were, however, less than those created by the standards.

Table 1a. Physical properties of the synthesized compounds.

Compounds	Found (Calcd)%M C H N S	Colour	Physical nature	Yield %	Melting points (^0C)	Conductivity $\Omega^{-1}cm^2 mol^{-1}$
MPH ($C_{11}H_{16}N_3SO$)	55.5 6.7 17.6 13.4 (55.4) (6.7) (17.3) (13.6)	White	Crystalline	48	268	0.72
$Fe(MPH)_2T_2$ $Fe[C_{30}H_{40}N_6 S_4O_2]$	8.0 51.4 5.7 12.0 18.3 (8.1) (50.9) (5.7) (12.4) (18.2)	Brown	Powdery	67	289	0.93
$Mn(MPH)_2T_2$ $Mn[C_{30}H_{40}N_6 S_4O_2]$	8.0 51.5 5.7 12.0 18.3 (8.1) (51.4) (5.7) (12.2) (18.2)	Pink	Powdery	56	272	0.75

Table 1b. Computed Results of antimicrobial assay.

Compounds	*S. aureus*	*E.coli*	*C. albicans*	*A. niger*
MPH	8	8	8	7
Mn-MPH)2T2	12	11	11	9
Fe-MPH)2T2	15	12	10	10
Ampiclox/ Fluconazole	25	22	22	23

3.1. Frontier molecular orbital (FMO)

A molecule's electron-donating and receiving ability can be defined using the value of the highest occupied molecular orbital (HOMO) and lowest unoccupied molecular orbital (LUMO) energy gap. These molecular orbitals play a vital role in electronic and optical properties, luminescence, photochemical reaction, UV-vis, quantum chemistry and pharmaceutical studies, and information about the biological mechanism [26,27]. HOMO-LUMO energy properties of the complex, such as hardness, softness, chemical potential, and electrophilicity index, are shown in Table 1. In contrast, the 3D plots for the HOMO and LUMO of the ligand and complexes are shown in Figure 3. The energy gap of one electron excitation from HOMO to LUMO for $Fe(MPH)_2T_2$ and $Mn(MPH)_2T_2$ is 3.39 eV and 2.83 eV, respectively. $FeMPH)_2T_2$ has the highest energy gap, which shows that it is a hard molecule. The lower energy gap of $Mn(MPH)_2T_2$ shows that it is softer and more reactive than $Fe(MPH)_2T_2$. A soft molecule is characterized by a low LUMO-HOMO energy gap, favoring better chemical reactivity and reflecting the compound's polarizability and hyperpolarizability. It requires less energy for excitation than $Fe(MPH)_2T_2$. Higher electron transitions occur in soft molecules than in hard molecules.

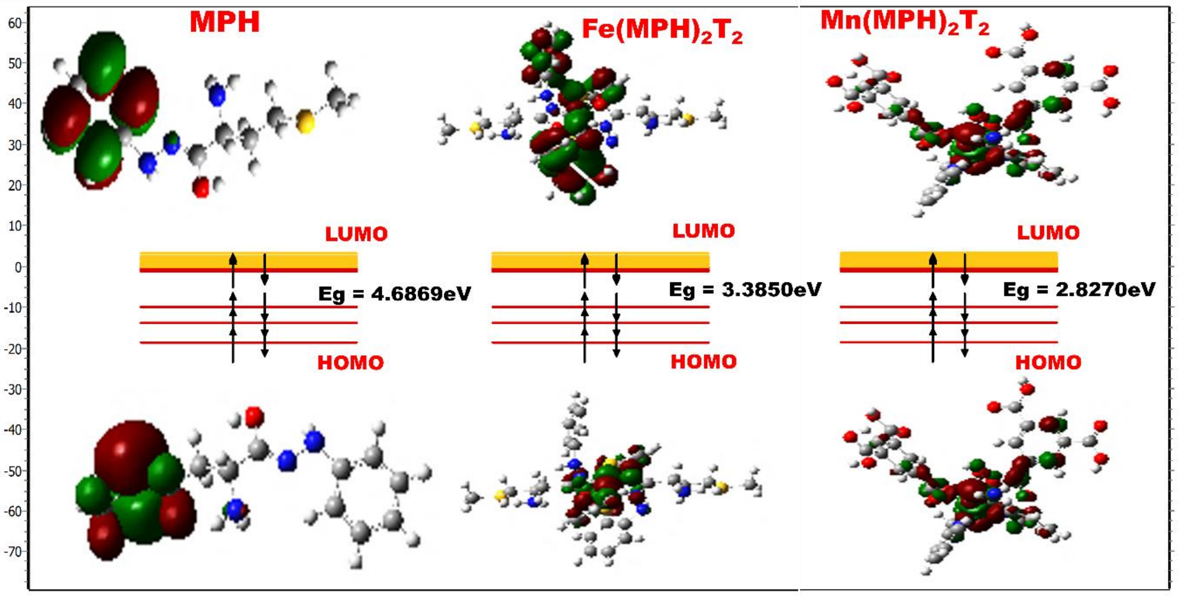

Figure 3. HOMO-LUMO diagram of methionine-phenylhradrazone-thiophene with Mn(II) and Fe(III) metal complexes

3.2. Population analysis

Mulliken atomic charges of the optimized structures were computed using the B3LYP/6-311++G (d,p) in the gas phase. The calculation of effective atomic charge plays a vital role in applying quantum mechanical calculation to molecular systems [28,29]. The total ($\sigma + \pi$) charge distribution in molecular or ionic species is a crucial parameter such as hydrogen bond acceptor ability and (dipole vs zwitterion) of the complexes [30,31]. The distribution of the Mulliken atomic charges is shown in Figure. S1(a)-(c) of the supporting information and from the results, the charges on O and N, atoms of the compound calculated by atomic dipole moment corrected Hirschfield population method (ADCH) and Mulliken population analysis method (MPA) are all negative and decreases respectively. This is because Oxygen with the highest value is more electronegative than all other atoms and can accept electrons freely and decreases down to Nitrogen atom and sulfur with the most negligible value and less electronegative. As a result, the bonds to sulfur are less polar than the corresponding bonds to N and O atoms [32]. The obtained values for the population analysis, including the Atomic dipole moment, corrected Hirshfield, and the Mulliken charges, were presented in Table SI (1)–(6) for a detailed understanding of charge analysis.

3.3. Global reactivity descriptors

The quantum chemical calculations were conducted to calculate the global reactivity electronic descriptors based on the well-known Koopmans approximation [33]. According to the approximation, the ionization potential and the electron affinity are approximately equal to the negative of the HOMO and LUMO energies, respectively.

$$IP = -E_{HOMO} \tag{1}$$

$$EA = -E_{LUMO} \tag{2}$$

Hence, the global reactivity descriptors could be computed using equations (3)-(6) as suggested in literature [34].

$$\chi = -\mu = \frac{IP+EA}{2} \tag{3}$$

$$\eta = {}^{1}/_{2}\,(IP - EA) = \frac{E_{LUMO}-E_{HOMO}}{2} \tag{4}$$

$$\omega = \frac{\mu^2}{2\eta} \tag{5}$$

$$S = \frac{1}{2\eta} = \frac{1}{IP-EA} = \frac{1}{E_{LUMO}-E_{HOMO}} \tag{6}$$

Where μ, χ, η, ω, and S are the chemical potential, electronegativity, chemical hardness, electrophilicity, and chemical softness, respectively. Molecules with smaller energy gap (E.g,) indicate softness, while molecules with more considerable energy gap exhibit hardness. Soft molecules are more reactive in comparison to hard molecules. As shown in Table 2, the Mn(MPH)2T2 complex has the lowest energy gap of 2.8276 eV, indicating its softness. The $Fe(MPH)_2T_2$ has a higher energy of 3.3856 eV gap, reflecting chemical hardness and suggesting that it is the hardest molecule. $Mn(MPH)_2T_2$ has the highest electrophilicity index of 92.18 eV, which indicates that it is the most electrophilic metal complex group [35]. Because both ω and EA evaluate an agent's ability to take electrons, it is expected that ö will be linked to EA. However, the electrophilicity index ω estimates the energy loss of a ligand due to maximum electron flow between donor and acceptor. In contrast, EA represents the ability to take only one electron from the environment [36].

Table 2. Quantum descriptors of the ligand and metal-ligand complexes.

Quantum descriptors	Ligand (MPH)	$Fe(MPH)_2T_2$ $Fe(C_{30}H_{40}N_6S_4O_2)$	$Mn(MPH)_2T_2$ $Mn(C_{30}H_{40}N_6S_4O_2)$
HOMO (eV)	-5.4618	-5.5445	- 11.7055
LUMO (eV)	-0.7749	-2.1589	-8.8779
Ionization potential IP (eV)	5.4618	5.5445	11.7055
Electron affinity EA (eV)	0.7749	2.1589	8.8779
Energy gap (E.g) (eV)	4.6869	3.3856	2.8276
hardness (Ƞ) (eV)	2.3433	1.6928	1.4138
Chemical potential (µ) (eV)	3.1184	6.6239	16.1445
Electrophilicity index (ω) (eV)	2.075	12.96	92.18
Electronegativity (χ) (eV)	3.118	3.851	10.29
Chemical softness (S) (eV)	0.213	0.295	0.354

3.4. Natural Bond Orbital (NBO)

It is efficient for studying intra and intermolecular bonding and interaction among bonds. It is also helpful for investigating charge transfer or conjugative interaction in molecular systems [37]. The larger the stabilization energy $E^{(2)}$ value, the greater the interaction between electron donors and the greater the extent of conjugation of the whole system.

Delocalization of electron density between occupied lewis type (bond or lone pair) NBO orbitals and unoccupied non-lewis NBO orbitals corresponding to a stable acceptor-donor interaction. Molecular interaction is formed by the orbital overlap between the σ(C-C) and σ* (C-C) Bond orbital, leading to intramolecular charge transfer. From the second order perturbation $E^{(2)}$ Theory, the donor NBO (i) and the acceptor NBO(j), the stabilization energy $E^{(2)}$ is related to the electron delocalization and acceptor by the equation.

$$E^{(2)} = qi\,\frac{(Fij))^2}{E(i)-E(j)} \qquad (7)$$

Where F_{ij} is the off-diagonal nature bond orbital fock matric elements, E(i) - E(j) is the diagonal elements, and qi is the orbital occupancy [36]. The perturbation energy of donor-acceptor interaction is presented in Table 3, while the optimized labeled structure is shown in Figure 4. In the ligand, the intramolecular interactions formed by the orbital overlap of $\sigma C_1 - C_2 \rightarrow \sigma^* C_3 - C_4$ has 21.09 kcal/mol, σC_1-$C_2 \rightarrow \sigma^* C_5$-$C_6$ has 20.15 kcal/mol and nπ- $N_{14} \rightarrow \sigma^* C_{15}$-$O_{24}$ has 17.33 kcal/mol which gives stronger stabilization to the structure. In the complex $Fe(MPH)_2T_2$, a conjugated ring form overlap between $\sigma C_{20} - C_{51}$ and $\sigma^* S_{49} - C_{51}$ with corresponding stabilization energy of 33.13 kcal/mol. At the same time, the Mn(II) complex gives stronger and greater stabilization energy of 55.75kj/mol at σC1 – C17 and σ*O61– H72, which is far greater than that of the ligand.

Table 3a. Second-order perturbation energy of MPH ligand.

Donor	Acceptor	E_2 (kcal/mol)	E_j - E_i	F (i,j)
σC_1-C_2	$\sigma^* C_3$-C_4	24.09	0.28	0.069
σC_1 - C_2	$\sigma^* C_5$-C_6	20.15	0.28	0.067
σC_1 - C_2	$\sigma^* C_3$-C_4	19.61	0.28	0.067
πC_{13}- N_{14}	$\sigma^* C_{15}$-O_{24}	17.33	0.63	0.094
πC_{15}– O_{24}	$\sigma^* N_{14}$-C_{15}	16.61	0.38	0.072
πC_{15} – O_{24}	$\sigma^* N_{14}$-C_{15}	15.41	0.38	0.072
πC_{15} – O_{24}	$\sigma^* N_{14}$-C_{15}	14.21	0.35	0.064
σC_{15} – C_{16}	$\sigma^* N_{12}$ - N_{14}	5.05	0.98	0.048
σC_{15} – C_{16}	$\sigma^* C_4$ - N_{14}	4.10	1.04	0.063
σC_{18} – H_{21}	$\sigma^* C_{16}$ – N_{26}	3.39	0.87	0.048

Table 3b. Second-order perturbation energy of the $Mn(MPH)_2T_2$.

Donor	Acceptor	E_2 (kcal/mol)	E_j - E_i	F (i,j)
σC_{20} – C_{51}	$\sigma^* S_{49}$ – C_{51}	33.13	0.90	0.169
σN_{16} – H_{17}	$\sigma^* S_{49}$ – C_{51}	27.61	1.27	0.168
σC_{20} – C_{51}	σC_{51} – H_{54}	23.92	1.12	0.160
σC_{20} – C_{51}	σC_{34} – H_{37}	22.71	1.41	0.158
σC_{21} – C_{23}	$\sigma^* C_{20}$ – C_{22}	21.17	0.28	0.066
$\sigma^* C_{21}$ – C_{23}	$\sigma^* C_{25}$ – C_{27}	19.91	0.28	0.066
σC_{33} – C_{81}	$\sigma^* S_{49}$ – C_{51}	17.48	0.87	0.110
σC_{33} – C_{81}	$\sigma^* C_{34}$ – H_{37}	15.35	1.11	0.117
σC_{33} – C_{81}	$\sigma^* C_{51}$ – H_{54}	13.11	1.09	0.107
σC_{36} – H_{39}	$\sigma^* C_{34}$ – H_{37}	12.12	0.93	0.095

Table 3c. Second-order perturbation energy of the $Mn(C_{30}H_{40}N_6S_4O_2)$.

Donor	Acceptor	E_2	E_j - E_i	F (ij)
σC_1– C_{17}	$\sigma^* O_{61}$ – H_{72}	55.75	1.24	0.235
σC_1– C_{17}	$\sigma^* C_4$ – H_8	48.92	1.91	0.247
σC_2 – C_3	$\sigma^* C_{21}$ – N_{75}	43.53	0.39	0.111

σC_2– N_{29}	σ * C_3–C_4	38.57	0.09	0.052
σC_1 – H_{17}	σ *C_{46}–O_{54}	37.69	1.68	0.234
σC_2 – C_3	σ *C_{28}–C_{83}	34.04	0.42	0.107
σC_1 – H_5	σ *C_{28} – H_{33}	28.10	0.25	0.076
σC_2– C_6	σ *C_{30} – H_{34}	19.75	0.09	0.037
σC_2– C_3	σ *C_{27} – C_{28}	17.24	0.55	0.090
σC_2– C_3	σ *C_{197}–N_{19}	11.09	0.26	0.048

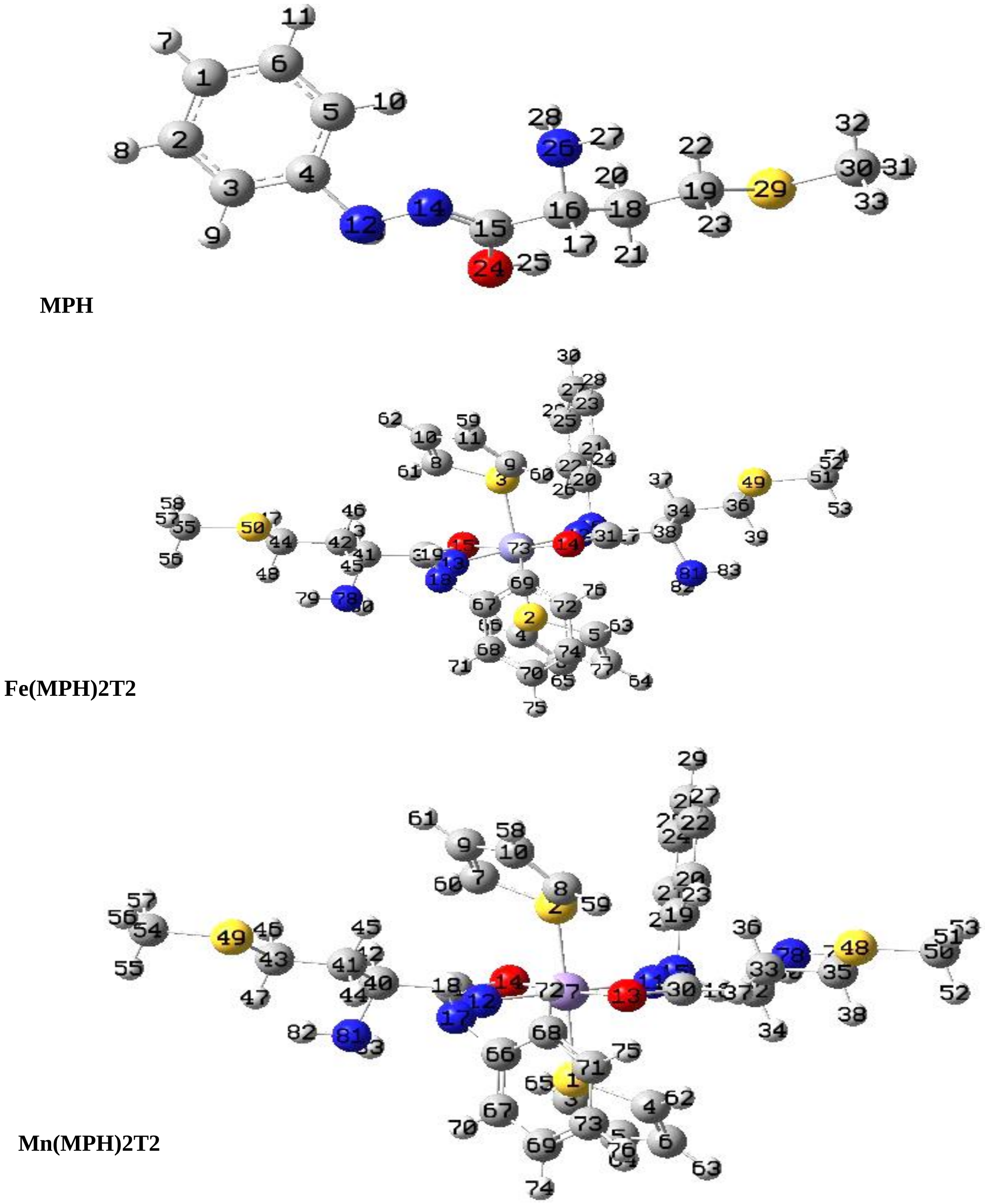

Figure 4. Optimized label diagram of the ligand (MPH), $Fe(MPH)_2T_2$, and $Mn(MPH)_2T_2$

3.5. Quantum theory of atoms-in-molecules (QTAIM)

The Bader's Theory QTAIM is a powerful tool used to investigate and explore the nature of chemical interactions between the ligand and the metal ions in the complexes based on electron density topology [37,38]. Bader's Theory can be used to analyze different types of weak interactive forces, such as the metal-metal interactions [39]. The nature of chemical interactions are evaluated in terms of electron density $\rho(r)$, the Laplacian of molecular electronic charge density ($\nabla^2\rho(r)$), the elliptical, Hessian eigenvalues, potential energy density V(r), Hamilton kinetic energy K(r), Lagrangian kinetic G(r) and total energy densities H(r) [40]. More information about the nature of interactions or bonds is obtained from the sign of the Laplacian of molecular electron charge density ($\nabla^2\rho(r)$. Greater electron density at critical bond points (BCPs) indicates greater structural stability [41]. A closed shell interaction found in ionic hydrogen bonds is defined by a positive $\nabla^2\rho(r)$ value at BCPs, while it negative value suggests shared interaction as covalent interactions [42]. The potential energy is dominant, and a negative charge is concentrated when the laplacian value is negative, while the kinetic energy dominates and the negative charge is depleted. If the laplacian value is positive, Cremer and Kraka have advocated that the total energy density H(r) is an important helpful parameter in describing the nature of chemical bonds or interaction [43]. The negative H(r) indicates a covalent interaction, while the positive shows an ionic interaction. In metal-ligand and metal-metal bonding, H(r) is usually negative and close to zero, whereas $\nabla^2\rho(r)>o$ at BCPs, positive and negative $\nabla^2\rho(r)$ values are indicative of closed-shell and shared electron interaction, respectively [44]. The topological parameters of the studied structures are shown in Table 4.

Three bonding patterns were outlined based on the value of potential energy density(V(r))/kinetic energy density(G(r)) [45]. If the V(r)/G(r)<2, then a shared-shell area of covalent bond is present. If V(r)/G(r)<2 it indicates a small number of covalent bonds or coordinate bonds [45]. The hydrogen bond energies can be computed using the formula by EHB = $1/2V_b$ where V_b is the potential energy density. The calculated values of ρ(r), $\nabla^2\rho(r)$, V(r), G(r), and H(r) for all the complexes under investigation are summarized in Tables 4(a) and (b). The values of electron density at critical bond point (BCP) for Fe complex is 0.0473 a.u and 0.0364 a.u from N_{32} - Fe_{38} and O_{22} - Fe_{38} concerning its Laplacian (0.1941 and 0.2225) at 78 and 82 BCP respectively. For Mn-complex, 0.06311a.u and 0.6030a.u were seen from O_{22} - Zn_{38} and N_{23} - Zn_{38} at 82 and 80 BCP respectively while its Laplacian is 0.3386 and 0.3110 respectively. Comparing the complexes, it is inferred that the Mn metal complex with the relatively highest coordination bond indicates a slight variation in their electron density at BCP. The negative value of H(r) indicates that the complexes' interaction and the ligand are electrostatic.

Table 4a. Results of the quantum theory of atoms-in-molecules for Fe-complex.

BOND	BCP	ρ(r)	G(r)	K (r)	H(r)	V(r)	$\Delta^2\rho(r)$
O_{22} – Fe_{38}	82	0.0364	0.0487	0.00691	-0.00691	-0.0417	0.2225
O_{23} – Fe_{38}	81	0.0713	0.1316	0.000053	-0.00005	-0.1317	0.5265
N_{32} –Fe_{38}	78	0.0473	0.0467	0.00181	-0.00181	-0.0449	0.1941
N_{33} –Fe_{38}	75	0.0464	0.0469	0.00205	-0.00205	-0.0448	0.1958

Table 4b. Results of the quantum theory of atoms-in-molecules for Mn-complex.

BOND	BCP	ρ(r)	G(r)	K (r)	H(r)	V(r)	$\Delta^2\rho(r)$
O_{35} –Mn_{38}	78	0.0546	0.0686	0.0085	-0.0085	-0.0771	0.2979
O_{22} –Mn_{38}	80	0.0631	0.0775	0.1077	-0.1077	-0.0177	0.3386
N_{23} -Mn_{38}	82	0.0563	0.0711	0.0088	-0.0088	-0.7998	0.3110
N_{33} -Mn_{38}	72	0.0439	0.0355	0.0101	-0.0101	-0.0456	0.1229

3.6. FT-IR analysis

The FT-IR is a Powerful tool for the assignments of functional group determination of compounds [46]. Infrared spectra were recorded within the range 370 cm^{-1} – 400 cm^{-1}. The selected infrared band in Table 5 gives the vibrational frequencies of relevant functional groups in the synthesized compounds. The bonds formed between the ligand and the metal ions were elucidated by comparing the spectra of the ligand with those of the complexes. A vibrational band with strong intensity at 3420 cm^{-1} assigned to ν(OH) stretching vibration disappeared due to deprotonation and coordination of the carbonyl oxygen to the metal ion [47,48]. The infrared spectrum of the ligand showed relatively strong bands at 3060 cm^{-1} to 3330 cm^{-1} attributed to $\nu(NH_2)$ and v(NH) stretching vibrations. In the spectra of the chelates, the frequency assigned to the NH_2 functional group is shifted to higher frequency values by 100 cm^{-1} – 300 cm^{-1} confirming the nitrogen bonding to the metal ion. The medium intensity band observed at 3280 cm^{-1} was assigned to v(NH), others at 930 cm^{-1} for (N-N) and 1020 cm^{-1} for (C-O). The band attributed to the azomethine group v(C=N) stretching vibration was observed at the spectra of the Fe(III) and Mn(II) complexes, respectively. The M-N band in the Fe and Mn complexes were seen at 503 cm^{-1} and 421 $cm^{-1,}$ while the M-S was at 391 cm^{-1} and 383 cm^{-1} and the M-O at 433 cm^{-1}, respectively. These observations were all in conformity with documented reports of [49]. The synthesized ligand's spectral and its complexes have been provided in Figures (S2)- (S4) with supporting information for better visualization.

Table 5. Infrared spectra of the ligand and metal complexes using KBr (cm^{-1}).

Compounds	v(OH)	v(C=N)	v(C-S)	v(M-N)	v(M-O)	v(M-S)
MPH	3322	1599	910	------	-------	------
$Fe(MPH)_2T_2$	3285	1536	844	509	435	391
$Mn(MPH)_2T_2$	3330	1535	844	421	429	383

3.7. Electronic Absorption Spectra

The electronic absorption spectra of the ligand (methioninephenylhydrazone) have three essential bands observed at 42,550 cm^{-1}, 38,462 $cm^{-1,}$ and 33, 680 cm^{-1}, each assignable to n-σ*, π- π* and n-π* transitions due to inter-ligand delocalization of electrons within the hetero-atoms and double bond network systems. In comparison with the theory, the UV-vis calculations conducted within the framework of time-dependent density functional theory (TD-DFT) reveal a maximum absorption band at 31164 $cm^{-1,}$ and the spectrum is reported in Figure (S5)-S(8) of the supporting information. This shows a strong agreement between theory and experiment. The weak bands of Mn(II) complex were observed at 16052 cm^{-1}, 23640 $cm^{-1,}$ and 29422 cm^{-1} assignable to ${}^6A_{1g} \rightarrow {}^4T_{1g}$, ${}^6A_{1g} \rightarrow {}^4T_{2g}$ transitions, including charge transfer, while the Fe(III) complex also displayed weak absorption bands at 12694 cm^{-1}, 18761 cm^{-1}, and 31250 cm^{-1} assignable to ${}^6A_{1g} \rightarrow {}^4T1_g$, ${}^6A_{1g} \rightarrow {}^4T_{1g}$, and charge transfer both attributable to octahedral configurations. These transitions occur in the molecules of the complexes but are shifted to lower intensities due to coordination to the metal ions due to d-d and charge transfer [50].

3.8. Nonlinear optics (NLO)

Nonlinear optics (NLO) studies light's inelastic and elastic deflection on the interaction of high-intensity lasers with a material. The literature has reported that a molecule's behavior can be affected by the interaction of electromagnetic fields in numerous areas [51]. The displaced charged particles generate polarization. Polarizability occurs when a dipole moment is induced in a material. Static polarizabilities are used to study the intramolecular and intermolecular interaction within the molecule. It is the initial response of the electron density to electric fields and accurately predicts the excited state treatment by density functional. The gaussian input file for the calculation was the previously optimized molecular geometries of the ligand, Fe(II), and Mn(II) complexes at the DFT/gen/B3LYP level of the computational method. The frequency-dependent electronic (hyper) polarizability and static polarizability β_{xyz} and α_{xyz} were computed using the coupled- Perturbed Hartree-Fock procedure. The basis set is suitable for computing the polarizabilities of molecules. Using the multi-win program, the output gaussian log file was used to calculate the NLO descriptors. The parameters obtained include; the dipole moments (μ), the polarizability anisotropies, the isotropically averaged polarizabilities ($\Delta\alpha$), and the isotropically first-order hyperpolarizabilities (βtotal), which were calculated using the formula below;

$$\mu = \sqrt{\mu 2x + \mu 2y + \mu 2z}, \tag{8}$$

$$\langle\alpha\rangle = \frac{1}{3}(\alpha xx + \alpha yy + \alpha zz), \tag{9}$$

$$\Delta\alpha_{\text{total}} = \{\tfrac{1}{2}[(\alpha xx - \alpha yy)^2 + (\alpha xx - \alpha zz)^2 + (\alpha yy - \alpha zz)^2 + 6(\alpha^2 xy + \alpha^2 xz + \alpha^2 yz)]\}^{1/2}, \tag{10}$$

$$\beta_{\text{total}} = \sqrt{\beta 2x + \beta 2y + \beta 2z}, \tag{11}$$

Where, $\beta_x = \beta_{xxx} + \beta_{xyy} + \beta_{xzz}$

$\beta_y = \beta_{yyy} + \beta_{xxy} + \beta_{yzz}$

$\beta_z = \beta_{zzz} + \beta_{xzz} + \beta_{yyz}$

The results of the NLO calculated properties of the studied compounds are presented in Table 6 for the ligand, Fe(II), and Mn(II), respectively. The results showed that the Fe(II) with the highest dipole moment (μ) of 6.41159, which is an indication of high charge separation and high electron density within the molecule. The first hyperpolarizability, which is a measure of the ease of inducement of a dipole in the presence of electricity, is highest in Mn(II) with a value of 9631.279 due to an increase in the volume of electrons ejected from the metal atom. The results of the NLO analysis predicted that the studied compounds or complexes are excellent candidates as NLO materials, the concept can be explained by means of the high charge separation. This result was compared with the related literature [52].

Table 6. The nonlinear optical properties of the studied compounds.

Dipole moment	**Value (D)**	**Static polarizability**	**Value (a.u)**	**Static hyperpolarizability**	**Value (a.u)**
Ligand (LG)					
X	-3.4465	αXX	-94.2424	βXXX	-97.2912
Y	1.4563	αXY	1.8815	βXXY	-6.5384
Z	1.0968	αYY	-95.1958	βXYY	-1.3080
μ	3.8989	αXZ	-9.1053	βYYY	21.7548
		αYZ	-0.9012	βXXZ	16.0864
		αZZ	-115.7917	βXYZ	-10.5140
		α_{TOTAL}	-203.57	βYYZ	15.4461
		Δα	95.12032	βXZZ	-12.6056
				βYZZ	7.9994
				βZZZ	-8.9858
				βX	-37.93431
				βY	584.4217
				βZ	99.6992
				β_{TOTAL}	594.677154
Fe(II) complex					
X	-2.4802	αXX	-289.9877	βXXX	-137.5844
Y	1.7484	αXY	-3.7122	βXXY	-25.9173
Z	-1.0699	αYY	-299.0473	βXYY	5.5796
μ	3.2176	αXZ	-19.4837	βYYY	37.2758
		αYZ	6.3080	βXXZ	12.3793
				βXYZ	5.9926
				βYYZ	0.8139
				βXZZ	-18.3471
				βYZZ	18.3087
				βZZZ	-27.2371
				βX	-635.527
				βY	-4088.48
				βZ	-1499.53
				β_{TOTAL}	4400.931
Mn(II) complex					
X	-2.4802	αXX	-289.9877	βXXX	-137.5844
Y	1.7484	αXY	-3.7122	βXXY	-25.9173

Z	-1.0699	αYY	-299.0473	βXYY	5.5796
μ	3.2176	αXZ	-19.4837	βYYY	37.2758
		αYZ	6.3080	βXXZ	12.3793
		αZZ	-265.6282	βXYZ	5.9926
		α_{TOTAL}	-203.57	βYYZ	0.8139
		Δα	95.12032	βXZZ	-18.3471
				βYZZ	18.3087
				βZZZ	-27.2371
				βX	209.72
				βY	-3815.43
				βZ	-41.96
				β_{TOTAL}	3821.42

3.9. Molecular docking

Molecular docking is an essential computational method in computer-aided drug design. It is a valuable tool for predicting a small molecule's most active binding site to its target protein [53]. The main purpose of molecular docking is to obtain an optimized conformation for each drug and protein with relative orientation between them such that the free energy of the overall system is minimized [54]. It is a computational tool and technique employed in predicting and evaluating the suitability of the studied compounds as a drug candidates. It is a method used to analyze molecules' orientation and conformation into the binding site of a macromolecular target. Toward this objective, comparative molecular docking was employed to study the drug delivery of the Schiff base and the complexes as a potential antibacterial drug candidate. The 3D crystallographic structures of the receptor molecules chosen for docking studies were achieved from the Protein Data Bank (PDB). The receptor proteins were prepared by removing water molecules, adding explicit hydrogens, Charges, and correcting deformation in the amino acid sequence. The active sites of the receptor protein were predicted and defined based on the interaction of the crystallographic ligand and the complexes with the receptor molecules as visualized with the discovery studio visualizer. The Schiff base and complexes were docked with two proteins: *E. coli* 2,2-dialkylglycine decarboxylase (PDB ID:1D7U) and *S. Aureus* DNA Gyrase (PDB ID:2XCS). The experimental results showed that the studied compounds have potential antimicrobial and antibacterial properties, which is why the two proteins 1D7U and 2XCS for molecular docking. From these docking results, Hydrogen bonding was not the only bonding type in the studied compounds. Other interactions like unfavorable Donor -Donor bond, pi cation, pi sigma, pi alkyl, salt bridge, and others can be seen in 2D and 3D with their respective bond distance. Using 2XCS as a receptor protein, the docking result obtained showed a binding affinity in the order Mn $(MPH)_2T_2$ > Fe $(MPH)_2T_2$ > MPH with binding affinities of -9.3, -8.4 and -7.1, respectively, while using 1D7U as the receptor, the binding relationship was observed to be Fe $(MPH)_2T_2$ > Mn $(MPH)_2T_2$ > MPH with the values -5.7, -5.3 and -5.2 respectively. It can be seen from these binding results that the Schiff base has the least binding affinity compared to the complexes. Generally, the binding relationship obtained showed that the studied receptors and the compounds have potential antimicrobial and antibacterial properties.

The docking results of the ligand (MPH), manganese (ii) ligand complex ($Mn(MPH)_2T_2$), and iron(iii) ligand complex ($Fe(MPH)_2T_2$), as well as the rooth, mean square distance of about the first mode is presented in Table 7. The ligand and the metal complexes generally showed more significant interaction with 2XCS protein compared to 1D7U, as can be seen from Table 7. More so, among the investigated synthesized complexes, Compound $Mn(MPH)_2T_2$ and $Fe(MPH)_2T_2$, exhibited Ki value for the 2XCS protein in the range of < micromolar. Thus, they can be considered a potential antibacterial agent and a drug candidate for managing bacteria diseases compared to the MPH ligand studied.

Table 7. Molecular docking results of the titled complexes concerning the receptor proteins of interest; 2xcs and 1d7u. $\boldsymbol{K}_{i=10}{}^{(Binding\ Affinity(B.A))}/_{(1.366)}$ [55]

Receptor protein	Complexes	Binding affinity (kcal/mol)	Rmsd (I.b)	Rmsd (u.b)	Inhibition constant (Ki (μM))
2xcs	MPH	-7.1	4.677	6.041	6.344
	$Mn(MPH)_2T_2$	-9.3	2.163	6.518	0.156
	$Fe(MPH)_2T_2$	-8.4	1.050	8.134	0.709
1d7u	MPH	-5.2	3.332	3.868	1.561
	$Mn(MPH)_2T_2$	-5.3	1.902	6.119	1.318
	$Fe(MPH)_2T_2$	-5.7	0.785	1.406	6.718

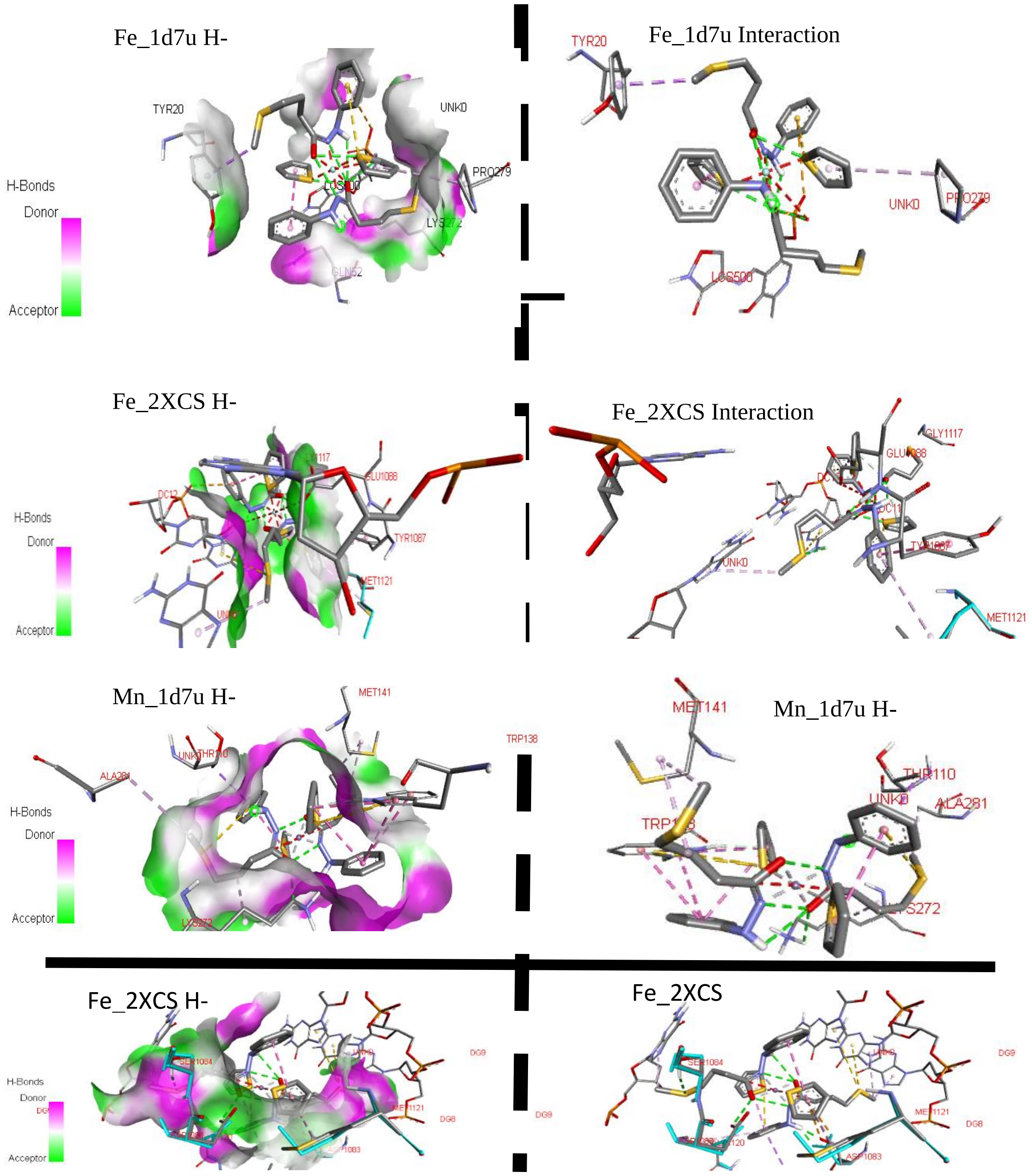

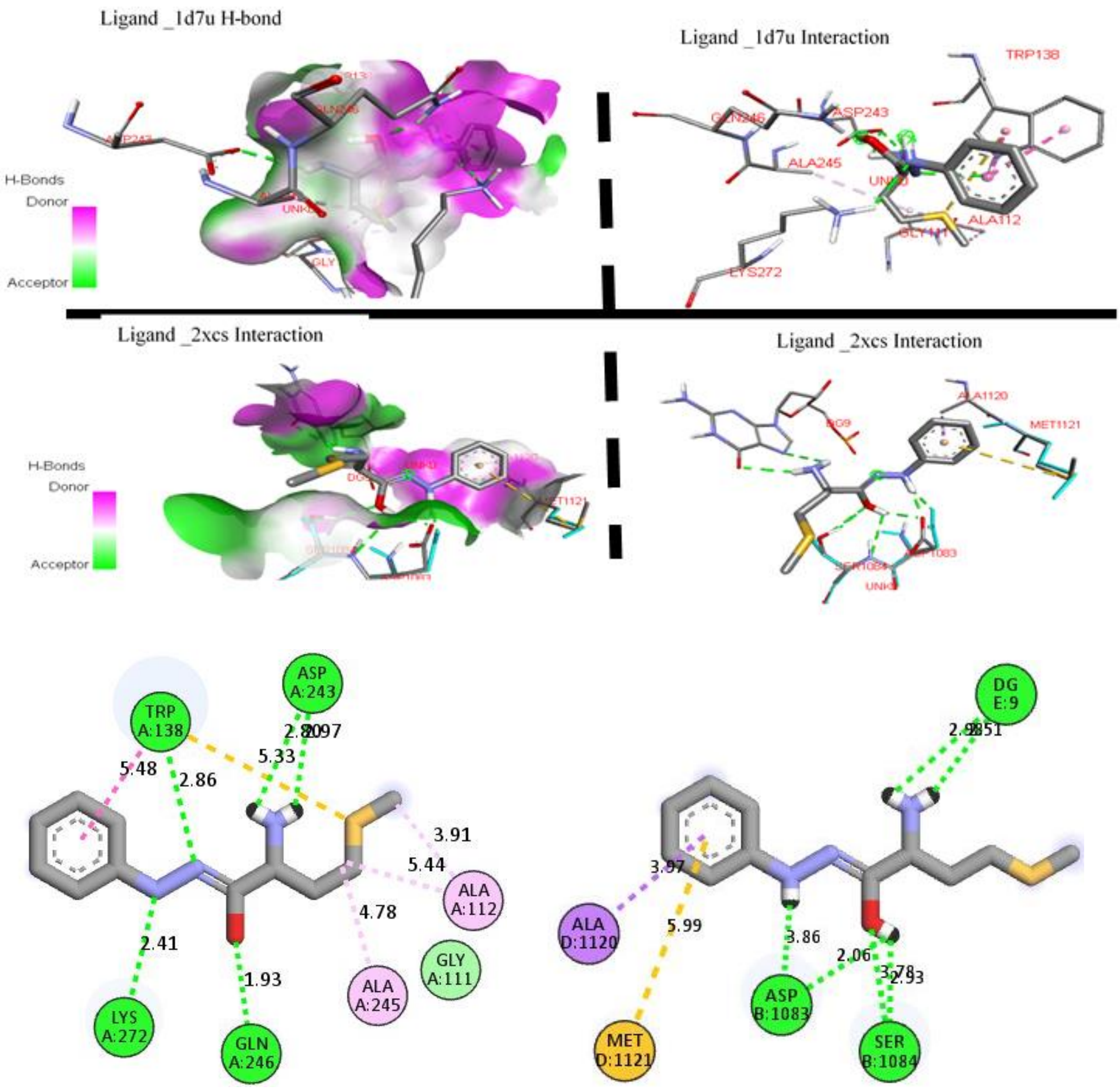

2D representation of the interaction between the ligand

4. Conclusions

Experimental and theoretical studies have been carefully evaluated on the mixed ligand complex of methionine-phenylhydrazone-thiophene and its Mn(II) and Fe(III) complexes. The compound reaction was first used to synthesize methionine and phenylhydrazine, considering thiophene as the secondary ligand. The experimental results were validated by theoretical calculation employing Density functional theory (DFT) using the gas phase as the medium for geometry optimization. From the analysis of HOMO – LUMO, the energy gap of the mixed ligand and its complexes were in the range 4.6869> 3.3856 > 2.8276 e/V, corresponding to MPH, $Fe(MPH)_2T_2$, and $Mn(MPH)_2T_2$ respectively which was an indication of the higher reactivity of $Mn(MPH)_2T_2$ compared to its congener. From the global quantum descriptor, considering the global electrophilicity index, the strongest electrophile was $Mn(MPH)_2T_2$ with 92.18 eV, while the weakest electrophile was $Fe(MPH)_2T_2$ with 3.118 eV. The NBO provided information on electron charge transfer within the system. . The Quantum Theory of Atoms- in- Molecules (QTAIM) showed the existence of a covalent bond network within the complexes. The FTIR spectra showed that the synthesized ligand was bidentate coordinating to the central metal through the azomethine nitrogen and the phenolic Oxygen and agreed with the theoretically calculated results. The complex had octahedral geometry. Molecular docking studies of the free ligand and its Mn(II) and Fe(III) complex showed that the complexes were more biologically active than the ligand with the binding affinity of -7.1, -9.3, -8.4 Kcal/mol for MPH, $Mn(MPH)_2T_2$ and $Fe(MPH)_2T_2$ respectively.

Availability of data and material

All data are contained in the Manuscript and Manuscript supporting information.

List of Abbreviations used in the Manuscript

ADCH	Atomic Dipole moment Corrected Hirschfield
a.u	Atomic Units.
B3LYP	Three parameters of Becke Lee Yang Parr
BCP	Bond Critical Point.
DFT	Density Functional Theory
EA	Electron Affinity
FT-IR	Fourier Transform Infrared
HOMO	Highest Occupied Molecular Orbital
IP	Ionization Potential
LUMO	Lowest Unoccupied Molecular Orbital
MPH	Methionine-phenylhydrazone
NBO	Natural Bond Orbital
NLO	Non-Linear Optics.
MPA	Mulliken Population Analysis
QTAIM	Quantum Theory of Atoms- in-Molecules
Rmsd	Rooth means square deviation.
TD-DFT	Time-Dependent Density Functional Theory
UV-vis	Ultraviolet Vis

Competing Interests

All authors declare zero conflict of interest.

Funding

This research did not receive funding from any source.

Authors Contribution

Terkumbur E. Gber and Innocent Benjamin: Project conceptualization, design, supervision, and administration. **Onyinye J. Ikenyirimba, Benjamin E. Etinwa, and Immaculata J. Ikot:** Writing, editing, analysis, and Manuscript draft. **Chioma M. Chima** Writing, editing, analysis. **Ismail O. Amodud and Imabasi T. Ita:** Writing and editing. **Bartholomew B. Isang and Grace Iniama**: Methodology, validation, and editing.

Acknowledgments

Any agency did not fund this research; however, the authors are thankful to all the Computational and Bio-simulation Research Group members at the University of Calabar.

References

1- W. Al Zoubi, A.A.S. Al-Hamdani, M. Kaseem, Synthesis and antioxidant activities of Schiff bases and their complexes: a review, Applied Organometallic Chemistry**, 2016**, 30, 810-817.

2- K. Prasad, C. Shivamallu, S. Gopinath, C. Srinivasa, C. Dharmashekara, P. Sushma, P. Ashwini, Schiff base ligands derived from 4-chloro-6-methylpyrimidin-2-amine: Chemical synthesis, bactericidal activity and molecular docking studies against targeted microbial pathogen, International Journal of Health & Allied Sciences, **2021**,10, 157-157.

3- M.N. Uddin, M.S. Amin, M.S. Rahman, S. Khandaker, W. Shumi, M.A. Rahman, S.M. Rahman, Titanium (IV) complexes of some tetra-dentate symmetrical bis-Schiff bases of 1, 6-hexanediamine: Synthesis, characterization, and in silico prediction of potential inhibitor against coronavirus (SARS-CoV-2), Applied organometallic chemistry, **2021**, 35, e6067.

4- S.H. Sherif, D.A. Kure, E.A. Moges, B. Argaw, Synthesis, Characterization and Antibacterial Activity Evaluation of 4-amino Antipyrine Derivatives and Their Transition Metal Complexes, American Journal of Bioscience and Bioengineering, **2021**, 9, 8-12.

5- S. Shaygan, H. Pasdar, N. Foroughifar, M. Davallo, F. Motiee, Cobalt (II) complexes with Schiff base ligands derived from terephthalaldehyde and ortho-substituted anilines: synthesis, characterization and antibacterial activity, Applied Sciences, **2018**, 8, 385.

6- R.K. Mohapatra, A.K. Sarangi, M. Azam, M.M. El-ajaily, M. Kudrat-E-Zahan, S.B. Patjoshi, D.C. Dash, Synthesis, structural investigations, DFT, molecular docking and antifungal studies of transition metal complexes with benzothiazole-based Schiff base ligands, Journal of Molecular Structure, **2019**, 1179, 65-75.

7- J.N. Laner, H.D.C.S. Junior, F.S., Rodembusch, E.C. Moreira, New insights on the ESIPT process based on solid-state data and state-of-the-art computational methods, Physical Chemistry Chemical Physics, **2021**, 23, 1146-1155.

8- J.F. Van der Maelen, J. Brugos, P. García-Álvarez, J.A. Cabeza, Two octahedral σ-borane metal (MnI and RuII) complexes containing a tripod κ3N, H, H-ligand: Synthesis, structural characterization, and theoretical topological study of the charge density, Journal of Molecular Structure, **2020**, 1201, 127217.

9- R. Kloditz, T. Radoske, M. Schmidt, T. Heine, T. Stumpf, M. Patzschke, Comprehensive Bonding Analysis of Tetravalent f-Element Complexes of the Type [M (salen) 2], Inorganic Chemistry, **2021**, 60, 2514-2525.

10- M. Sathish, L. Rajasekaran, D. Shanthi, N. Kanagathara, S. Sarala, S. Muthu, Spectroscopic (FT-IR, FT-Raman, UV-Vis) molecular structure, electronic, molecular docking, and thermodynamic investigations of indole-3-carboxylic acid by DFT method, Journal of Molecular Structure, **2021**, 1234, 130182.

11- J.M. Vicent-Luna, S. Apergi, S. Tao, Efficient Computation of Structural and Electronic Properties of Halide Perovskites Using Density Functional Tight Binding: GFN1-xTB Method, Journal of chemical information and modeling, **2021**, 61, 4415-4424.

12- M. Kaneko, S. Nakashima, Density Functional Theory Study on the 193Ir Mössbauer

Spectroscopic Parameters of Vaska's Complexes and Their Oxidative Adducts, Inorganic Chemistry, **2021**, 60, 12740-12752.
13- A. Abdou, Synthesis, Structural, Molecular Docking, DFT, Vibrational Spectroscopy, HOMO-LUMO, MEP Exploration, antibacterial and antifungal activity of new Fe (III), Co (II) and Ni (II) hetero-ligand complexes, Journal of Molecular Structure, **2022**, 1262, 132911.
14- A. Abdou, H.M. Mostafa, A.M.M. Abdel-Mawgoud, seven metal-based bi-dentate NO azocoumarine complexes: Synthesis, characterization, DFT calculations, Drug-Likeness, in vitro antimicrobial screening and molecular docking analysis, Inorganica Chimica Acta, **2022**, 121043.
15- G.E. Iniama, T.I. Iorkpiligh, Spectral characterization and antimicrobial studies of synthesized Fe (III) and Mn (II) mixed ligand complexes of methioninephenylhydrazone with thiophene, World Wide J. Multidisc. Res. and Development, **2018**, 4(9), 1-5.
16- G.G. Mohamed, Z.H. Abd El-Wahab, Mixed ligand complexes of bis (phenylimine) Schiff base ligands incorporating pyridinium moiety: Synthesis, characterization and antibacterial activity, Spectrochimica Acta Part A: Molecular and Biomolecular Spectroscopy, **2005**, 61, 1059-1068.
17- Y.S. Priya, K.R. Rao, P.V. Chalapathi, A. Veeraiah, K.E. Srikanth, Y.S. Mary, R. Thomas, Intricate spectroscopic profiling, light harvesting studies and other quantum mechanical properties of 3-phenyl-5-isooxazolone using experimental and computational strategies, Journal of Molecular Structure, **2020**, 1203, 127461.
18- N. Siddiqui, S. Javed, Quantum computational, spectroscopic investigations on ampyra (4-aminopyridine) by DFT/TD-DFT with different solvents and molecular docking studies, Journal of Molecular Structure, **2021**, 1224, 129021.
19- H. Louis, I.B. Onyebuenyi, J.O. Odey, A.T. Igbalagh, M.T. Mbonu, E.A. Eno, O.E. Offiong, Synthesis, characterization, and theoretical studies of the photovoltaic properties of novel reactive azonitrobenzaldehyde derivatives, RSC Advances, **2021**, 11, 28433-28446.
20- J.A. Agwupuye, H. Louis, O.C. Enudi, T.O. Unimuke, M.M. Edim, Theoretical insight into electronic and molecular properties of halogenated (F, Cl, Br) and hetero-atom (N, O, S) doped cyclooctane, Materials Chemistry and Physics, **2022,** 275, 125239.
21- N. Pandey, M.S. Mehata, S, Pant, N, Tewari, Structural, Electronic and NLO Properties of 6-aminoquinoline: A DFT/TD-DFT Study, Journal of Fluorescence, **2021**, 31, 1719-1729.
22- H. Louis, T.E. Gber, F.A. Asogwa, E.A. Eno, T.O. Unimuke, V.M. Bassey, B.I. Ita, Understanding the lithiation mechanisms of pyrenetetrone-based carbonyl compound as cathode material for lithium-ion battery: Insight from first principal density functional theory, Materials Chemistry and Physics, **2021**, 125518.
23- S. Şahin, N. Dege, Synthesis, Characterization, X-Ray, HOMO-LUMO, MEP, FT-IR, NLO, Hirshfeld surface, ADMET, Boiled-Egg Model Properties and Molecular Docking Studies with Human Cyclophilin D (CypD) of a Schiff Base Compound:(E)-1-(5-nitro-2-(piperidin-1-yl) phenyl)-N-(3-nitrophenyl) methanimine, Polyhedron, **2021**, 115320.
24- I.C. Carvalho, H.S. Mansur, A.A. Mansur, S.M. Carvalho, L.C.A. de Oliveira, M. de Fatima Leite, Luminescent switch of polysaccharide-peptide-quantum dot nanostructures for targeted-intracellular imaging of glioblastoma cells, Journal of Molecular Liquids, **2020**, 304, 112759.
25- J.A. Agwupuye, P.A. Neji, H. Louis, J.O. Odey, T.O. Unimuke, E.A. Bisiong, T.N. Ntui, Investigation on electronic structure, vibrational spectra, NBO analysis, and molecular docking studies of aflatoxins and selected emerging mycotoxins against wild-type androgen receptor, Heliyon, **2021**, 7, e07544.
26- S. Muthu, J.U. Maheswari, Quantum mechanical study and spectroscopic (FT-IR, FT-Raman, ^{13}C, ^{1}H, UV) study, first order hyperpolarizability, NBO analysis, HOMO and LUMO analysis of 4-[(4-aminobenzene) sulfonyl] aniline by ab initio HF and density functional method, Spectrochimica Acta Part A: Molecular and Biomolecular Spectroscopy, **2012**, 92, 154-163.
27- L. Li, C. Wu, Z. Wang, L. Zhao, Z. Li, C. Sun, T. Sun, Density functional theory (DFT) and natural bond orbital (NBO) study of vibrational spectra and intramolecular hydrogen bond interaction of l-ornithine–l-aspartate, Spectrochimica Acta Part A: Molecular and Biomolecular Spectroscopy, **2015**, 136, 338-346.
28- E.A. Eno, H. Louis, T.O. Unimuke, T.E. Gber, I.J. Mbonu, C.J. Ndubisi, S.A. Adalikwu, Reactivity, stability, and thermodynamics of para-methylpyridinium-based ionic liquids: Insight from DFT, NCI, and QTAIM, Journal of Ionic Liquids, **2022**, 100030.
29- T.O. Unimuke, H. Louis, E.A. Eno, E.C., Agwamba, A.S. Adeyinka, Meta-Hybrid Density Functional Theory Prediction of the Reactivity, Stability, and IGM of Azepane, Oxepane, Thiepane, and Halogenated Cycloheptane, ACS omega, **2022**, 7, 13704-13720.
30- V.M. Bassey, C.G. Apebende, P.S. Idante, H. Louis, W. Emori, C.R. Cheng, F.C. Asogwa, Vibrational Characterization and Molecular Electronic Investigations of 2-acetyl-5-methylfuran using FT-IR, FT-Raman, UV–VIS,

NMR, and DFT Methods, Journal of Fluorescence, **2022**, 1-13.

31- A.D. Udoikono, H. Louis, E.A. Eno, E.C. Agwamba, T.O. Unimuke, A.T. Igbalagh, A.S. Adeyinka, Reactive azo compounds as a potential chemotherapy drug in the treatment of malignant glioblastoma (GBM): Experimental and theoretical studies, Journal of Photochemistry and Photobiology, **2022**, 10, 100116.

32- E.A. Eno, J.I. Mbonu, H. Louis, F.S. Patrick-Inezi, T.E. Gber, T.O. Unimke, O.E. Offiong, Antimicrobial activities of 1-phenyl-3-methyl-4-trichloroacetyl-pyrazolone: Experimental, DFT studies, and molecular docking investigation, Journal of the Indian Chemical Society, **2022**,100524.

33- T. Rohand, H. Ben EL Ayouchia, H. Achtak, A. Ghaleb, Y. Derin, A. Tutar, K. Tanemura, Design, synthesis, DFT calculations, molecular docking and antimicrobial activities of novel cobalt, chromium metal complexes of heterocyclic moiety-based 1, 3, 4-oxadiazole derivatives, Journal of Biomolecular Structure and Dynamics, **2021**, 1-14.

34- U.J. Undiandeye, H. Louis, T.E. Gber, T.C. Egemonye, E.C., Agwamba, I.A. Undiandeye, B.I. Ita, Spectroscopic, conformational analysis, structural benchmarking, excited state dynamics, and the photovoltaic properties of Enalapril and Lisinopril, Journal of the Indian Chemical Society, **2022**, 100500.

35- H. Louis, O.I. Amodu, T.O. Unimuke, T.E. Gber, B.B. Isang, A.S. Adeyinka, Modeling of $Ca_{12}O_{12}$, $Mg_{12}O_{12}$, and Al12N12 nanostructured materials as sensors for phosgene (Cl_2CO)." Materials Today Communications, **2022**, 103946.

36- J.A. Agwupuye, H. Louis, T.O. Unimuke, P. David, E.I. Ubana, T.L. Moshood, Electronic structure investigation of the stability, reactivity, NBO analysis, thermodynamics, and the nature of the interactions in methyl-substituted imidazolium-based ionic liquids, Journal of Molecular Liquids, **2021**, 337, 116458.

37- A. Suvitha, N.S. Venkataramanan, Trapping of organophosphorus chemical nerve agents by pillar [5] arene: A DFT, AIM, NCI and EDA analysis, Journal of Inclusion Phenomena and Macrocyclic Chemistry, **2017**, 87, 207-218.

38- H. Yang, P. Boulet, M.C. Record, A rapid method for analyzing the chemical bond from energy densities calculations at the bond critical point, Computational and Theoretical Chemistry, **2020**, 1178, 112784.

39- M. Usman, R.A. Khan, A. Alsalme, W. Alharbi, K.H. Alharbi, M.H. Jaafar, S. Tabassum, Structural, Spectroscopic, and Chemical Bonding Analysis of Zn (II) Complex [Zn (sal)](H2O): Combined Experimental and Theoretical (NBO, QTAIM, and ELF) Investigation, Crystals, **2020**,10, 259.

40- O.C. Enudi, H. Louis, M.M. Edim, J.A. Agwupuye, F.O. Ekpen, E.A. Bisong, P.M. Utsu, Understanding the aqueous chemistry of quinoline and the diazanaphthalenes: insight from DFT study, Heliyon, **2021**, 7, e07531.

41- D.K. Miller, C. Loy, S.V. Rosokha, Examining a Transition from Supramolecular Halogen Bonding to Covalent Bonds: Topological Analysis of Electron Densities and Energies in the Complexes of Bromosubstituted Electrophiles, ACS omega, **2021**, 6, 23588-23597.

42- E.C. Agwamba, A.D. Udoikono, H. Louis, E.U. Udoh, I. Benjamin, A.T. Igbalagh, U.B. Ushaka, Synthesis, characterization, DFT studies, and molecular modeling of azo dye derivatives as a potential candidate for trypanosomiasis treatment, Chemical Physics Impact, **2022**,100076.

43- A.U. Agobi, H. Louis, A.J. Ekpunobi, T.O. Unimuke, A.I. Ikeuba, A.M. Pembere, C.N. Ozoemena, Theoretical investigation of the structural, optoelectronic, and the application of waste graphene oxide/polymer nanocomposite as a photosensitizer, Materials Research Express, **2022**, 9, 065301.

44- K. Velmurugan, R. Vickram, C.V. Jipsa, R. Karthick, G. Prabakaran, S. Suresh, R. Nandhakumar, Quinoline based reversible fluorescent probe for Pb^{2+}; applications in milk, bioimaging and INHIBIT molecular logic gate, Food Chemistry, **2021**, 348, 129098.

45- L.G. Ferreira, R.N. Dos Santos, G. Oliva, A.D. Andricopulo, Molecular docking and structure-based drug design strategies, Molecules, **2015**, 20, 13384-13421.

46- Q.S. Obu, H. Louis, J.O. Odey, I.J. Eko, S. Abdullahi, T.N. Ntui, O.E. Offiong, Synthesis, Spectra (FT-IR, NMR) investigations, DFT study, in silico ADMET and Molecular docking analysis of 2-amino-4-(4-aminophenyl) thiophene-3-carbonitrile as a potential anti-tubercular agent, Journal of Molecular Structure, **2021**, 130880.

47- A. Abdou, O.A. Omran, A. Nafady, I.S. Antipin, Structural, spectroscopic, FMOs, and nonlinear optical properties exploration of three thiacaix (4) arenes derivatives, Arabian Journal of Chemistry, **2022**,15, 103656.

48- N. Nagasundaram, K. Padmasree, S. Santhosh, V. Vinoth, N. Sedhu, A. & Lalitha, Ultrasound promoted synthesis of new azo fused dihydropyrano [2, 3-c] pyrazole derivatives: In vitro antimicrobial, anticancer, DFT, in silico ADMET and Molecular docking studies, Journal of Molecular Structure, **2022**,1263, 133091.

49- K. Wei, H. Louis, W. Emori, P.S. Idante, E.C. Agwamba, C.R. Cheng, T.O. Unimuke, Antispasmodic activity of carnosic acid extracted from Rosmarinus officinalis: Isolation, spectroscopic characterization, DFT studies, and in silico molecular docking investigations, Journal of Molecular Structure, **2022**,1260, 132795.

50- A. Lawal, A.S. Shodeinde, S.A Amolegbe, S.E. Elaigwu, M.T. Yunus-Issa, Synthesis, Characterization and Antimicrobial Activity of Mixed Transition Metal Complexes of Salicylic with 1,10- phenanthroline, Journal of Appl. Sci. Environ.Mange, **2017**, 21, 568-573.
51- A. Abdou, O.A. Omran, A. Nafady, I.S. Antipin, Structural, spectroscopic, FMOs, and nonlinear optical properties exploration of three thiacaix (4) arenes derivatives, Arabian Journal of Chemistry, **2022**,15, 103656.
52- N.A. Elkanzi, A. Ali, H. Hrichi, A. Abdou, New mononuclear Fe (III), Co (II), Ni (II), Cu (II), and Zn (II) complexes incorporating 4-{[(2 hydroxyphenyl) imino] methyl} phenyl-4-methylbenzenesulfonate (HL): Synthesis, characterization, theoretical, anti-inflammatory, and molecular docking investigation, Applied Organometallic Chemistry, **2022**, 36, e6665.
53- F.C. Asogwa, E.C. Agwamba, H. Louis, M.C. Muozie, I. Benjamin, T.E. Gber, A. I. Ikeuba, Structural Benchmarking, Density Functional Theory Simulation, Spectroscopic Investigation and Molecular Docking of N-(1H-pyrrol-2-yl) methylene)-4-methylaniline as Castration-Resistant Prostate Cancer Chemotherapeutic Agent, Chemical Physics Impact, **2022**, 100091.
54- E.A. Eno, F.A. Patrick-Inezi, H. Louis, T.E. Gber, T.O. Unimuke, E.C. Agwamba, S.A. Adalikwu, Theoretical investigation and antineoplastic potential of Zn (II) and Pd (II) Complexes of 6-Methylpyridine-2-carbaldehyde-N (4)-ethylthiosemicarbazone, Chemical Physics Impact, **2022**,100094.
55- A. Abdou, A.M.M. Abdel-Mawgoud, Synthesis, structural elucidation, and density functional theory investigation of new mononuclear Fe (III), Ni (II), and Cu (II) mixed-ligand complexes: Biological and catalase mimicking activity exploration, Applied Organometallic Chemistry, **2022**, 36, e6600.